Inorg. Chem. **2007**, *46*, 3851–3855

Structure and Magnetic Properties of $Pb_2Cu_3B_4O_{11}$: a New Copper Borate Featuring $[Cu_3O_8]^{10-}$ Units

Shilie Pan,[†] Byron Watkins,[‡] Jared P. Smit,[†] Michael R. Marvel,[†] Ian Saratovsky,[†] and Kenneth R. Poeppelmeier*,[†]

Department of Chemistry, Northwestern University, 2145 Sheridan Road, Evanston, Illinois 60208-3113, and Department of Physics and Astronomy, Northwestern University, 2145 Sheridan Road, Evanston, Illinois 60208-3112

Received August 7, 2006

$Pb_2Cu_3B_4O_{11}$ crystallizes in the monoclinic space group *P*2/*n* (No. 13) with $a = 6.8016(15)$ Å, $b = 4.7123(10)$ Å, $c = 14.614(3)$ Å, $\beta = 97.089(3)°$, and $Z = 2$. The crystal structure consists of infinite $[Cu_3O_8]^{10-}$ zigzag chains of alternating dimers and monomers. The magnetic susceptibility and specific heat capacity show spin-gap and Curie–Weiss behaviors that can be explained by a model of Cu(2)–Cu(2) dimers and isolated or weakly coupled Cu(1) monomers.

Introduction

Mixed-metal oxides that contain copper dimers or trimers have received considerable attention, owing to their interesting magnetic properties.[1−10] For example, $La_4Cu_3MoO_{12}$ is an isolated Heisenberg triangle spin trimer model,[2,3] in which the antiferromagnetic intratrimer interactions are frustrated. $A_3Cu_3(PO_4)_4$ with A = Ca, Sr, or Pb is a model system of the linear Heisenberg antiferromagnetic $S = 1/2$ trimer.[4] $SrCu_2(BO_3)_2$ is a model system of isolated spin dimers.[8] These phases display unique spin interactions and spin exchange pathways.

The exchange pathways in extended structures can be complex, and it is important to understand these pathways for device applications. Understanding spin exchange dynamics contributes to the basic knowledge of chemical bonds, which in turn leads to new and improved materials, for example, nanoscale materials for magnetic memory.

An extensive search of the $PbO-CuO-B_2O_3$ system has led to a new phase, $Pb_2Cu_3B_4O_{11}$. In the current work, the interesting magnetic properties are reported and current models are adapted to discuss the spin exchange interactions. The synthesis, crystal structure, vibrational spectroscopy, magnetic susceptibility, and specific heat capacity of $Pb_2Cu_3B_4O_{11}$ are reported.

Experimental Section

Synthesis. Polycrystalline $Pb_2Cu_3B_4O_{11}$ was prepared in a platinum crucible by solid-state reaction method using stoichiometric ratios of PbO (99.99%, Alfa-Aesar), CuO (99.995%, Alfa-Aesar), and B_2O_3(99.98%, Sigma-Aldrich). The mixture was heated slowly from room temperature to 600 °C in air for 2−3 days with intermittent grinding. The sample purity was verified using X-ray powder diffraction.

X-ray powder diffraction analysis of $Pb_2Cu_3B_4O_{11}$ was performed at room temperature in the angular range of $2\theta = 10-70°$ with a scan step width of 0.02° and a fixed counting time of 1 s/step using an automated Rigaku X-ray diffractometer equipped with a diffracted-beamed monochromator set for Cu Kα ($\lambda = 1.5418$ Å) radiation. The experimental powder X-ray diffraction pattern of Pb_2-

* To whom correspondence should be addressed. E-mail: krp@northwestern.edu.
† Department of Chemistry.
‡ Department of Physics and Astronomy.

(1) Vander Griend, D. A.; Boudin, S.; Caignaert, V.; Poeppelmeier, K. R.; Wang, Y.; Dravid, V. P.; Azuma, M.; Takano, M.; Hu, Z.; Jorgensen, J. D. *J. Am. Chem. Soc.* **1999**, *121*, 4787.
(2) Azuma, M.; Odaka, T.; Takano, M.; Vander Griend, D. A.; Poeppelmeier, K. R.; Narumi, Y.; Kindo, K.; Mizuno, Y.; Maekawa, S. *Phys. Rev.* **2000**, *62B*, R3588.
(3) Qiu, Y.; Broholm, C.; Ishiwata, S.; Azuma, M.; Takano, M.; Bewley, R.; Buyers, W. J. L. *Phys. Rev.* **2005**, *71B*, 214439/1.
(4) Matsuda, M.; Kakurai, K.; Belik, A. A.; Azuma, M.; Takano, M.; Fujita, M. *Phys. Rev.* **2005**, *71B*, 144411/1.
(5) Mo, X.; Etheredge, K. M. S.; Hwu, S-J.; Huang, Q. *Inorg. Chem.* **2006**, *45*, 3478.
(6) Ranmohotti, K. G. S.; Mo, X.; Smith, M. K.; Hwu, S-J. *Inorg. Chem.* **2006**, *45*, 3665.
(7) Anderson, J. B.; Kostiner, E.; Ruszala, F. A. *J. Solid State Chem.* **1981**, *39*, 29.
(8) Kageyama, H.; Onizuka, K.; Yamauchi, T.; Ueda, Y.; Hane, S.; Mitamura, H.; Goto, T.; Yoshimura, K.; Kosuge, K. *J. Phys. Soc. Jpn.* **1999**, *68*, 1821.
(9) Belik, A. A.; Matsuo, A.; Azuma, M.; Kindo, K.; Takano, M. *J. Solid State Chem.* **2005**, *178*, 709.
(10) Sakurai, H.; Yoshimura, K.; Kosuge, K.; Ishikawa, F.; Mitamura, H.; Goto, T. *J. Phys. Soc. Jpn.* **2002**, *71*, 664.

10.1021/ic0614824 CCC: $37.00
Published on Web 04/12/2007

$Cu_3B_4O_{11}$ is in agreement with the calculated data based on the single-crystal data, suggesting that it is pure phase (Figures S1 and S2 in the Supporting Information).

Crystal Growth. A covered platinum crucible containing a 1:1:1 molar ratio of PbO, CuO, and B_2O_3 was placed into the center of a vertical, programmable temperature Molysili furnace. The furnace was heated to a temperature of 970 °C at a rate of 10 °C /min, maintained for 24 h, cooled to 600 °C at a rate of 0.1 °C /min, and finally cooled to room temperature at a rate of 10 °C /min. Blue platelike crystals were separated from the melt for the structure determination.

X-ray Crystallographic Studies. A plate-shaped blue single crystal of $Pb_2Cu_3B_4O_{11}$ with the dimensions 0.01 × 0.13 × 0.60 mm^3 was chosen for the structure determination. Unit cell parameters were derived from a least-squares analysis of 3124 reflections in the range $3.48° < \theta < 29.03°$ on a Bruker SMART − 1000 CCD diffractometer using monochromatic Mo Kα radiation (λ = 0.71073 Å) and integrated with the SAINT-Plus program.[11]

All calculations were performed with programs from the SHELXTL crystallographic software package.[12] The space group *P*2/*n* was determined unambiguously from the systematic absences, and the structure was solved by direct methods. A face-indexed absorption correction was performed using the XPREP program, followed by the SADABS program;[13] equivalent reflections were then averaged. Final least-squares refinement on F_0^2 with data having $F_0^2 \geq 2\sigma(F_0^2)$ includes anisotropic displacement parameters for all atomic positions. The final difference Fourier synthesis may have shown maximum and minimum peaks at 4.165 (0.85 Å from Pb_1) and −4.045 e/Å^3 (0.81 Å from Pb_1), respectively. Additional crystal data and structure refinement information are summarized in Table 1.

Vibrational Spectroscopy. The mid-infrared spectrum was obtained at room temperature via a Bio-Rad FTS-60 FTIR spectrometer. The sample was mixed thoroughly with dried KBr (5 mg of the sample, 500 mg of KBr), and the spectrum was collected in a range from 400 to 4000 cm^{-1} with a resolution of 2 cm^{-1}.

Differential Thermal Analysis. Differential thermal analysis (DTA) was performed under static air on a TA Instruments, Inc. differential thermal analyzer 1600-2910 DSC. The sample and reference (Al_2O_3) were enclosed in Pt crucibles, heated from room temperature to 970 °C, and then cooled to room temperature at a rate of 10 °C/min.

Magnetic and Specific Heat Measurements. Direct current (dc) magnetic susceptibility ($\chi = M/H$) was measured on a Quantum Design MPMS5 Superconducting Quantum Interference Device (SQUID) magnetometer in the temperature ranges 2−300 and 4−400 K in an applied field of 500 Oe under both zero-field-cooled (ZFC) and field-cooled (FC) conditions. Specific heat capacity, C_p, versus temperature, *T*, of $Pb_2Cu_3B_4O_{11}$ was recorded between 2 and 300 K at zero magnetic field and at 9 T by a pulse relaxation method using a Quantum Design PPMS calorimeter.

Results and Discussion

Crystal Structure. Final atomic coordinates and equivalent isotropic displacement parameters are listed in Table 2, and selected interatomic distances and angles are given in Table S1 in the Supporting Information.

Table 1. Crystal Data and Structure Refinement for $Pb_2Cu_3B_4O_{11}$

empirical formula	$Pb_2Cu_3B_4O_{11}$
temperature	153(2) K
wavelength	0.71073 Å
formula weight	824.24
crystal system	monoclinic
space group	*P*2/*n*
unit cell dimens	$a = 6.8016(15)$ Å $\alpha = 90°$ $b = 4.7123(10)$ Å $\beta = 97.089(3)°$ $c = 14.614(3)$ Å $\gamma = 90°$
volume	464.82(17) Å^3
Z	2
density (calcd)	5.889 g/cm^3
absorption coefficient	42.908 /mm
F(000)	718
cryst size	0.01 × 0.13 × 0.60 mm^3
θ range for data collection	3.48−29.03°
index ranges	$-8 \leq h \leq 9$ $-6 \leq k \leq 6$ $-19 \leq l \leq 18$
reflns collected	3645
independent reflns	1124 [*R*(int) = 0.0400]
completeness to $\theta = 29.03$	89.7%
max and min transmission	0.64373 and 0.01355
refinement method	full-matrix least-squares on F^2
data/restraints/params	1124/0/94
GOF on F^2	1.120
final *R* indices [$I > 2\sigma(I)$][a]	R1 = 0.0345, wR2 = 0.0940
R indices (all data)[a]	R1 = 0.0386, wR2 = 0.0965
extinction coefficient	0.0018(5)
largest diff. peak and hole	4.165 and −4.045 e/Å^3

[a] $R1 = \sum||F_o| - |F_c||/\sum|F_o|$ and $wR2 = [\sum w(F_0^2 - F_c^2)^2/\sum wF_0^4]^{1/2}$ for $F_0^2 > 2\sigma(F_0^2)$ and $w^{-1} = \sigma^2(F_0^2) + (0.0651P)^2 + 0.1985P$ where $P = (F_0^2 + 2F_c^2)/3$.

Table 2. Atomic Coordinates (×10^4) and Equivalent Isotropic Displacement Parameters (Å^2 × 10^3) for $Pb_2Cu_3B_4O_{11}$[a]

atom	Wyckoff position	x	y	z	U_{eq}
Pb(1)	4*g*	−156(1)	4288(1)	6913(1)	8(1)
Cu(1)	2*d*	0	0	5000	7(1)
Cu(2)	4*g*	3493(2)	4815(2)	5586(1)	7(1)
B(1)	4*g*	−3677(17)	−510(19)	5945(8)	8(2)
B(2)	4*g*	2957(15)	9980(20)	6604(7)	8(2)
O(1)	4*g*	−1880(12)	757(13)	5874(5)	14(2)
O(2)	2*f*	2500	1236(18)	7500	8(2)
O(3)	4*g*	1784(9)	1856(12)	5913(4)	8(1)
O(4)	4*g*	2482(10)	7058(12)	6487(5)	13(1)
O(5)	4*g*	−4896(11)	631(11)	6574(5)	9(1)
O(6)	4*g*	5724(9)	7090(12)	5479(4)	10(1)

[a] U_{eq} is defined as one-third of the trace of the orthogonalized U_{ij} tensor.

The structure of $Pb_2Cu_3B_4O_{11}$ is depicted in Figure 1. There is one unique lead site, two unique copper sites, two unique boron sites, and six unique oxygen sites in the asymmetric unit (see Table 2). The coordination of lead is a distorted PbO_5 square pyramid. The oxygen atoms fall within the same hemisphere around lead, owing to the $6s^2$ lone electron pair of Pb^{2+} in the opposite direction (see Figure 1). The coordination environment around the PbO_5 structure unit is shown in Figure S3 in the Supporting Information. PbO_5 units are surrounded by three separate BO_4 tetrahedra and two separate BO_3 trigonal planar groups. The PbO_5 polyhedron shares edges with four different atoms (Cu(1), Cu(2), B(2) (twice)). The lead atom shares two oxygen atoms (edges) with both Cu(1) and Cu(2) with O(3) common to the $Pb(1)O_5$, $Cu(1)O_4$, and $Cu(2)O_4$ polyhedra. Additionally, Pb(1) shares edges with B(2) in two distinct ways. $Pb(1)O_5$

(11) *SAINT-Plus*, version 6.02A; Bruker Analytical X-ray Instruments, Inc.: Madison, WI, 2000.
(12) Sheldrick, G. M. *SHELXTL*, version 6.14; Bruker Analytical X-ray Instruments, Inc.: Madison, WI, 2003.
(13) *Bruker SMART*, version 5.054; *SADABS*, version 2.05; Bruker Analytical X-ray Systems, Inc.: Madison, WI, 2003.

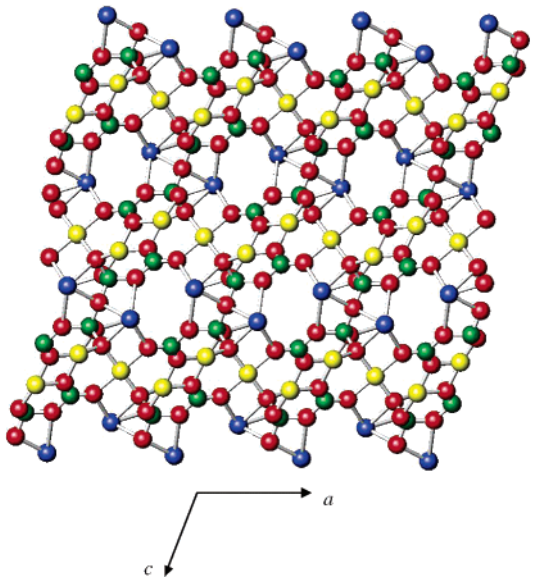

Figure 1. Structure of $Pb_2Cu_3B_4O_{11}$. The blue spheres are Pb, the yellow spheres are Cu, the green spheres are B, the red spheres are O. Lead and boron polyhedra are separated by chains of CuO_4 polyhedra.

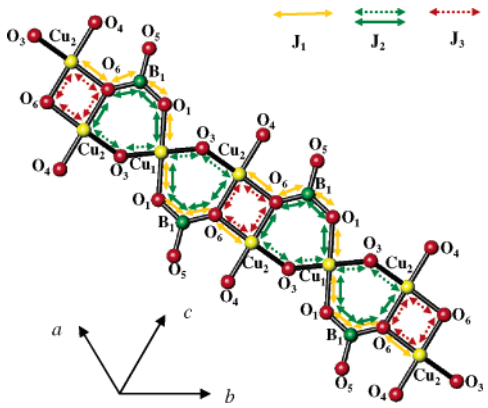

Figure 2. Connectivity of the CuO_4 polyhedra. The yellow spheres are Cu, the red spheres are O, and the green spheres are B. Infinite zigzag chains are formed by $[Cu_3O_8]^{10-}$ units. The J_1, J_2, and J_3 interactions are shown.

is linked to $B(2)O_4$ by both O(3) and O(2) forming one edge, as well as by O(5) and O(2) forming the other edge.

The copper atoms exhibit two distinct coordination CuO_4 polyhedra. Cu(1) is surrounded by four oxygen atoms forming a regular rectangular plane, while Cu(2) has a slightly distorted rectangular coordination. Important for understanding the magnetic spin interactions, which are discussed later, are the infinite zigzag chains of $[Cu_3O_8]^{10-}$ units that are shown in Figure 2. The chains can be viewed as Cu(2)−Cu(2) dimers that share O(3) atoms as corners with Cu(1) monomers. Alternatively, the chains can be viewed as Cu_3O_8 trimers, where the $Cu(1)O_4$ rectangular plane is linked by O(3) on each side by $Cu(2)O_4$ polyhedra.

The boron atoms also exhibit two distinct coordination polyhedra. B(1) shows a trigonal planar oxygen coordination, while B(2) forms a BO_4 tetrahedron. The connectivity of the boron−oxygen polyhedra is shown in Figure 3. Corner-sharing BO_4 dimers are bordered by BO_3 trigonal planar groups and together form discrete B_4O_{11} tetramers.

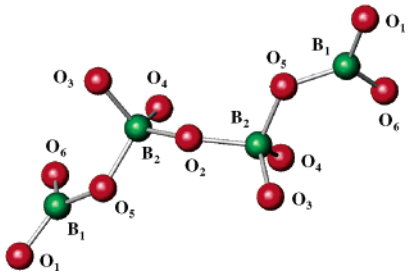

Figure 3. Connectivity of boron−oxygen polyhedra. The green spheres are B, the red spheres are O. Corner-sharing BO_4 dimers are bordered by BO_3 trigonal planar groups, forming isolated B_4O_{11} tetramers.

The bond valence sums of each atom in $Pb_2Cu_3B_4O_{11}$ were calculated[14,15] and are listed in Table 3. These charges, based on the bond lengths determined by the X-ray structure analysis, are in agreement with the expected oxidation states.

Vibrational Spectroscopy. IR spectroscopy was carried out with the objective of specifying and comparing the coordination of boron in $Pb_2Cu_3B_4O_{11}$, and the spectrum from 400 to 4000 cm^{-1} is shown in Figure S4 in the Supporting Information. The absorptions in IR spectrum of the synthetic sample were assigned on the basis of results obtained from vibrational spectra measurements of other borate groups.[16−19] The main infrared absorption region between about 1200 and 1400 cm^{-1} reveals two absorption bands, owing to stretching of trigonal BO_3 (1239 cm^{-1}) and tetrahedral BO_4 (1279 cm^{-1}) groups, respectively. The bands at 1025, 876, 821, and 779 cm^{-1} are likely the asymmetric and symmetric stretching of B−O in BO_4. In the long-wavelength part of the spectrum there are weak bands at 466, 590, and 659 cm^{-1} which correspond to the deformation vibrations of the atoms in boron−oxygen polyhedra. The remaining bands in the spectrum are likely attributed to Cu−O and Pb−O vibrations.

Thermal Stability. The DTA curve of $Pb_2Cu_3B_4O_{11}$ is shown in Figure S5 in the Supporting Information. The sample began to decompose at 671 °C, and further decomposition occurs at 818 °C, suggesting that $Pb_2Cu_3B_4O_{11}$ melts incongruently. In order to further verify that $Pb_2Cu_3B_4O_{11}$ melts incongruently, 0.8 g of $Pb_2Cu_3B_4O_{11}$ powder was heated to 970 °C and cooled to room temperature. Analysis of the powder XRD pattern of the melt revealed that the diffraction pattern is different from that of the initial $Pb_2Cu_3B_4O_{11}$ powder (Figure S6 in the Supporting Information), which further suggests that $Pb_2Cu_3B_4O_{11}$ is an incongruently melting compound.

Magnetic Susceptibility. Two interpretations of the spin exchange paths in $Pb_2Cu_3B_4O_{11}$ are presented. The first interpretation views the $[Cu_3O_8]^{10-}$ unit as a dimer and a monomer and is presented in the text. The second interpretation views the $[Cu_3O_8]^{10-}$ unit as a trimer and is presented in the Supporting Information. The dimer and monomer model fits the data well numerically and conceptually. The

(14) Brown, I. D.; Altermatt, D. *Acta Crystallogr.* **1985**, *41B*, 244.
(15) Brese, N. E.; O'Keeffe, M. *Acta Crystallogr.* **1991**, *47B*, 192.
(16) Pisarski, W. A.; Pisarska, J.; Ryba-Romanowski, W. *J. Mol. Struct.* **2005**, *744−747*, 515.
(17) Liu, Z.; Li, L.; Li, J.; Hu, M. *J. Alloys Comp.* **2005**, *394*, 277.
(18) Liu, Z.; Zuo, C.; Hu, M. *Thermochim. Acta* **2005**, *435*, 168.
(19) Liu, Z.; Li, S.; Zuo, C. *Thermochim. Acta* **2005**, *433*,196.

Table 3. Bond Valence Analysis of the $Pb_2Cu_3B_4O_{11}$[a,b]

atom	O(1)	O(2)	O(3)	O(4)	O(5)	O(6)	$\Sigma_{cations}$
Pb(1)	0.400	[×2]0.479	0.485	0.506	0.156		2.026
Cu(1)	0.482[×2]		0.547[×2]				2.058
Cu(2)			0.531	0.575		0.581 + 0.510	2.197
B(1)	0.987				0.881	1.041	2.909
B(2)		[×2]0.700	0.715	0.874	0.709		2.998
Σ_{anions}	1.869	2.358	2.278	1.955	1.746	2.132	

[a] Bond valences calculated with the program Bond Valence Calculator Version 2.00, Hormillosa, C., Healy, S., Stephen, T. McMaster University (1993). [b] Valence sums calculated with the formula: $S_i = \exp[(R_0 - R_i)/B]$, where S_i = valence of bond "i" and $B = 0.37$. Left and right superscripts indicate the number of equivalent bonds for anions and cations, respectively.

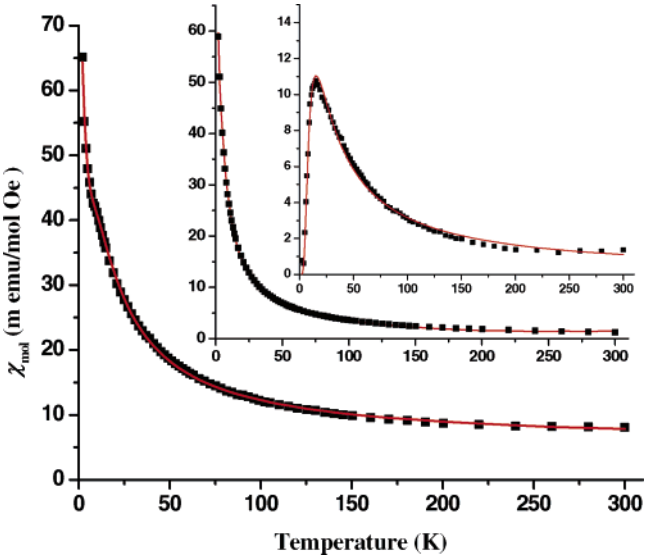

Figure 4. Spin-dimer plus monomer model of magnetic response for $Pb_2Cu_3B_4O_{11}$. The bottom graph shows the combined fit, the middle graph shows the Curie−Weiss fit, and the top graph shows the dimer fit.

trimer model also numerically fits the low-temperature anomaly in susceptibility, better than the dimer-plus-monomer model, but provides no cause for the observed large paramagnetic background.

As mentioned above, the crystal structure consists of infinite $[Cu_3O_8]^{10-}$ zigzag chains of alternating dimers and monomers linked by oxygen superexchange paths and oxygen−boron−oxygen super-superexchange paths. J_1 and J_2 in Figure 2 are the interactions between dimer and monomer; J_3 in Figure 2 is the intradimer interaction and is responsible for the spin gap (Δ).

The bottom curve in Figure 4 depicts the χ_{mol} vs T curve for $Pb_2Cu_3B_4O_{11}$. The magnetic susceptibility curve deviates from the standard Curie−Weiss behavior in the range 7 K $< T <$ 50 K, implying the formation of a spin gap. The spin-gap hypothesis is supported by the fact that the magnetic susceptibility curve shows a shoulder around 12 K. Spin-gap behavior is plausible in this compound because $Pb_2Cu_3B_4O_{11}$ has a Cu(2)−Cu(2) dimer (J_3 in Figure 2) similar to that in $SrCu_2(BO_3)_2$, which is an orthogonal dimer system with a spin-gap ground state.[8,20,21] Since J_3 is the intradimer interaction and the copper atoms of the dimer are in close proximity, J_3 is likely to be dominant. A spin-gap ground state owing to an antiferromagnetic J_3 can then cause the anomaly in the magnetic susceptibility at 12 K while the Cu(1) monomer causes the Curie−Weiss response. If J_3 dominates J_1 and J_2 in $Pb_2Cu_3B_4O_{11}$, the infinite chain can be considered as Cu(2)−Cu(2) dimers and isolated or weakly coupled Cu(1) monomers. Because this is a reasonable possibility, the susceptibility data were modeled by chains of alternating dimers and monomers:[8,20,21]

$$\chi = \chi_0 + \frac{N_A {\mu_B}^2}{k_B}\left[\frac{{g_M}^2 S(S+1)}{3(T-\theta)} + \frac{{g_D}^2}{T(3+\exp(\Delta/T))}\right] \quad (1)$$

where χ_0 gives the temperature-independent term; g_M, g_D, N_A, μ_B, and k_B are monomer g-factor, dimer g-factor, Avogadro's number, the Bohr magneton, and Boltzmann constant, respectively. The first bracketed term gives the Curie−Weiss response of the monomers (with spin $S = 1/2$), and the last term gives the spin-gap (Δ) response of the dimers. The magnetic susceptibility as a function of temperature can be fit well by this model, and the deviations are similar to those observed by others.[8,20,21] The curve fitting is shown in Figure 4. The best-fit gives $g_M = 2.01$, $g_D = 1.90$, $\chi_0 = 5.47 \times 10^{-3}$ emu/mol·K, $\theta = -4.4$ K, $\Delta/k_B = 24.6$ K. The critical temperature in the Curie−Weiss law ($\theta = -4.4$ K) agrees well with the transition in the heat capacity discussed later, which is ascribed to magnetic impurities and/or defects on Cu^{2+} sites in $Pb_2Cu_3B_4O_{11}$.

The bottom curve in Figure 4 represents the original susceptibility data (squares) and the best fit to eq 1 (line). Similarly, the middle curve is the Curie−Weiss portion of the data and the monomer fit and the top curve is the spin-gap data and the dimer fit. The values of data (squares) for the monomer (middle) and dimer (top) contributions were obtained by subtraction from the original susceptibility and were computed and are plotted as the lines in the graphs. The spin gap is evident from the vanishing of dimer susceptibility (top) at low temperature. One should note from the form of the fitted function that the monomers contribute 1/3 of the spins and the dimers contribute 2/3 of the spins.

As suggested by one reviewer, magnetic susceptibility was remeasured from 4 to 400 K (Figure S8 in the Supporting Information). Measurements up to 800 K would give valuable information. If the susceptibility increases with increasing temperature at higher temperature, it would suggest the presence of a large spin gap. However, the instrument is

(20) Kageyama, H.; Yoshimura, K.; Stern, R.; Mushnikov, N. V.; Onizuka, K.; Kato, M.; Kosuge, K.; Slichter, C. P.; Goto, T.; Ueda, Y. *Phys. Rev. Lett.* **1999**, *82*, 3168.
(21) Sebastian, S. E.; Yin, D. .; Tanedo, P.; Jorge, G. A.; Harrison, N.; Jaime, M.; Mozharivskyj, Y.; Miler, G.; Krzystek, J.; Zvyagin, S. A.; Fisher, I. R. *Phys. Rev.* **2005**, *71B*, 212405/1.

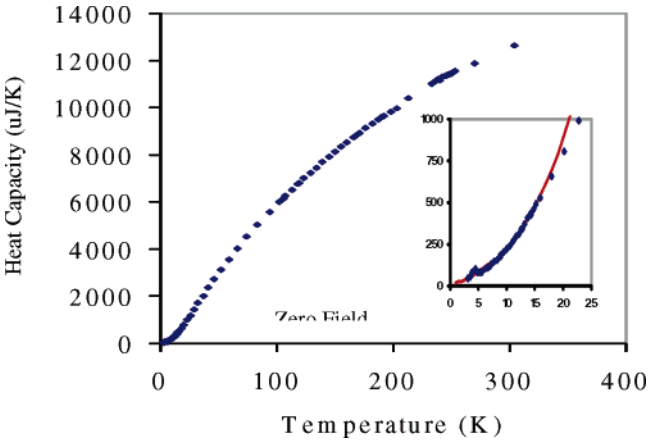

Figure 5. Specific heat measurement for $Pb_2Cu_3B_4O_{11}$ in zero magnetic field. Inset gives the C_p vs T curve between 2 and 20 K.

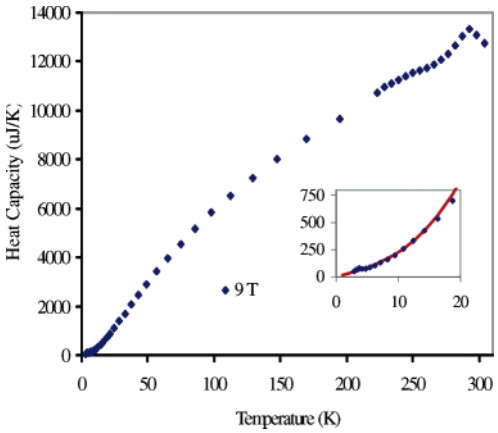

Figure 6. Specific heat measurement for $Pb_2Cu_3B_4O_{11}$ in 9 T field. Inset gives the C_p vs T curve between 2 and 20 K.

limited to a maximum temperature of 400 K. Therefore, data were fit by the Curie−Weiss Law from 50 to 200 K, the dimer contribution was neglected in this temperature range, and a Curie term of 2/3 was obtained. The observed susceptibility likely is not due to the unpaired Cu(2) spins alone because a value of 1/3 would be expected in this case.

Specific Heat. Figure 5 shows the variation of the specific heat for $Pb_2Cu_3B_4O_{11}$ in zero magnetic field, as a function of temperature between 2 and 300 K. The specific heat measurement for $Pb_2Cu_3B_4O_{11}$ shows a λ-type anomaly at ~4 K, which is ascribed to magnetic impurities and/or defects of Cu^{2+} ions. Additionally, the specific heat measurement in 9 T field between 2 and 300 K shows another anomaly at 290 K, as shown in Figure 6 (the anomaly at 4 K is unaffected by the field). No clear cause for the peak at 290 K in 9 T field is evident in this model, but it has been verified that it reproduces itself. It is possible that closer inspection will reveal similar results in $H = 0$ specific heat observations.

Figure 7 shows graphs of C_{mag}/T vs T and of S_{mag} vs T (magnetic heat capacity and magnetic entropy, respectively). The magnetic heat capacity was obtained by fitting the heat capacity data from 7 to 15 K to the form $C_p = aT + bT^3 + cT^5$ to obtain a reasonable representation of lattice, electronic, and nuclear heat capacities combined. This representation was then extrapolated to zero temperature and subtracted pointwise from our data. The result was then divided by the

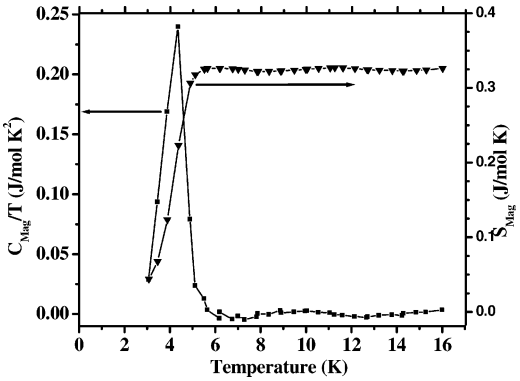

Figure 7. Graphs of C_{mag}/T vs T and of S_{mag} vs T.

sample temperature (C_{mag}/T) and integrated (S_{mag}) to yield the points on the graphs. The oscillatory behavior in these graphs is the results of the polynomial model. The magnetic entropy is 330 mJ/mol·K above 6 K. This value is far too small to reflect ordering in the monomers and/or dimers, so the peak can be ascribed to the presence of impurities.

Conclusions

The structure of $Pb_2Cu_3B_4O_{11}$ is built up from infinite zigzag chains of $[Cu_3O_8]^{10-}$ units, and it is possible to view these chains as alternating dimers and monomers. From the analysis of magnetic susceptibility and heat capacity, $Pb_2Cu_3B_4O_{11}$ has spin-gap and Curie−Weiss behavior, and the Cu(2)−Cu(2) spin dimer is the origin of the spin gap, while the Cu(1) monomer is the origin of Curie−Weiss response.

Acknowledgment. We gratefully acknowledge the support from the National Science Foundation (Solid State Chemistry Awards No. DMR-0312136 and DMR-0604454), the EMSI program of the National Science Foundation at the Northwestern University Institute for Environmental Catalysis (Grant No. 9810378), and the Department of Engergy, BES-Chemical Sciences, Geosciences, and Biosciences Division under Grant No. DE-FG0203ER15457, and the use of the Central Facilities supported by the MRSEC program of the National Science Foundation (DMR-0520513) at the Materials Research Center of Northwestern University. We especially thank the reviewers for their valuable comments.

Supporting Information Available: An X-ray crystallographic file in CIF format including crystallographic details, atomic coordinates, interatomic distances and angles; calculated X-ray diffraction pattern data; observed X-ray diffraction pattern data of $Pb_2Cu_3B_4O_{11}$ before and after melting; differential thermal analysis plot; an infrared spectrum; trimer model; remeasured SQUID data to 400 K. This material is available free of charge via the Internet at http://pubs.acs.org.

IC0614824